Submillimeter-Scale Combustion

Craig M. Miesse and Richard I. Masel
Dept. of Chemical and Biomolecular Engineering, University of Illinois, Urbana IL 61801

Craig D. Jensen
Delphi Corporation, Troy, MI 48098

Mark A. Shannon
Dept. of Mechanical and Industrial Engineering, University of Illinois, Urbana IL 61801

Mark Short
Dept. of Theoretical and Applied Mechanics, University of Illinois, Urbana IL 61801

DOI 10.1002/aic.10271
Published online in Wiley InterScience (www.interscience.wiley.com).

Until recently, the concept of combustion within a confined space defined by a microburner was thought to be impossible. Extensive literature dating back to Davy's seminal work in 1817 has discussed how thermal and chemical quenching set a minimum size below which no flame can exist. In this report, though, it is shown that microcombustion is possible if the wall composition and structure are carefully controlled. It is suggested that there are three keys to obtaining microcombustion: (1) the walls of the microburner need to be fabricated from materials that do not quench radicals so that the gas-phase combustion reactions can occur unimpeded; (2) the device needs to be insulated well enough that the net heat generation is sufficient to keep the reacting mixture hot enough to sustain significant combustion; and (3) the flow pattern in the burner needs to be such that the temperature is low enough not to melt the walls, yet the flame fills the entire space. Using this design strategy, devices burning methane–air and propane–air mixtures in a 750-μm slot were designed and optimized to achieve high conversion. These results show that microcombustion is possible with consideration of microscale engineering challenges and fitting combustor design.
AIChE J, 50: 3206–3214, 2004

Introduction

Since Davy (1817) demonstrated that flames are quenched passing through a fine wire gauze, it has been widely accepted that the homogeneous combustion of hydrocarbon fuels at atmospheric pressures cannot generally be sustained below a critical reactor dimension, usually of the order of a few millimeters (for example, Kuo, 1986). This is primarily attributed to two effects: as the combustion vessel decreases in size, the surface-to-volume ratio increases, resulting both in increased combustor surface heat loss and increased potential destruction of radical intermediates at the walls (Fernandez-Pello, 2002). However, because of the appeal of the high energy density of hydrocarbon fuels, there has been substantial interest in developing microcombustion as a power source in micromechanical devices such as microengines and as heat sources for microfuel converters.

The objective of this article is to summarize recent work from our laboratory. In a previous paper Jensen et al. (2003) showed that sustained combustion is possible, although unfor-

Correspondence concerning this article should be addressed to R. I. Masel at r-masel@uiuc.edu.

tunately Jensen et al.'s burners were not robust: they failed after 8 h. Here we will provide designs of robust burners. We will also provide data to show that the structure of flames in submillimeter burners is fundamentally different from the structure of flames on a larger scale.

Over the last 5 years, the field of microscale combustion has been advancing through the feasibility stage. In addition to the development of enabling miniature-scale fabrication techniques for microcombustion, research into the physical engineering challenges of microcombustion is also under way. There are many consequences of decreasing the length scale of propagating flames. As the length scale of a combustion channel is decreased, the surface area-to-volume ratio increases approximately inversely with the critical dimension. As a result, the influence of interfacial phenomena is amplified. Detrimentally, the two dominant mechanisms of flame quenching, thermal and radical quenching, are interfacial in nature. *Thermal quenching* of confined flames occurs when heat generated by the combustion process fails to keep pace with the heat loss to the walls. The walls effectively act as an enthalpy sink for the homogeneous combustion zone, lowering the temperature and retarding the kinetic mechanisms, further reducing heat generation and leading to flame extinction. *Radical quenching*, the second interfacial phenomenon between the gas-phase reaction zone and the solid wall interface, is a heterogeneous kinetic process whereby highly reactive radical intermediates undergo termination reactions at the wall. The removal of these radicals, crucial to the propagation of homogeneous catalytic cycles in the combustion mechanism, quenches the flame. Both quenching mechanisms act to reduce the reaction rates of the homogeneous reactions. For microcombustion processes to benefit from the high conversion typical of combustion reactions, diffusion times and reaction times must be greater than reactor residence times. However, as the length scale decreases, the Reynolds number for the flow decreases, until only laminar flow is possible. Laminar flow eliminates turbulent mixing, thus increasing diffusion times. Concurrently, feed velocities for the combustion processes do not scale with reactor length, resulting in lower residence times. Thus, in addition to flame quenching issues, microcombustion is further challenged by conversion concerns. Note that at the length scale of interest, on the order of hundreds of micrometers, conventional assumptions regarding fluid behavior apply. The gap dimensions are sufficiently greater than the mean free paths of the molecules so that no-slip conditions and continuum models are appropriate.

In spite of these challenges, the interest in submillimeter combustion has increased as the micropower generation (MPG) and micro-electromechanical system (MEMS) fields have evolved. Successfully harnessing the specific energies of hydrocarbons for power generation could contribute to revolutionizing the portable power industry and could enable a host of innovative devices.

In the research presented here, our goal is to determine whether gas-phase microcombustion of hydrocarbon fuels can be achieved in a small burner, and to characterize the performance of such a device. Our approach was to (1) find materials of construction that do not quench radicals; (2) build a burner out of these materials, (3) insulate the burner well enough so that the heat generated by the gas-phase combustion would be sufficient to maintain the wall temperature above 1000°C [because Lucquin (1964) shows that the methane combustion rate increases rapidly at 800–1000°C]; and (4) characterize the burner's performance. In practice, the analysis in Masel (1996) was used to identify several candidate wall materials that are not expected to trap radicals. The materials were then tested by mounting two parallel plates of the materials on a movable assembly, passing a flame through the plates, and then gradually reducing the gap between the plates until the flames quench. Such a procedure allowed materials that did not quench flames to be identified. Fully enclosed burners were also developed, constructed of a well-performing material in the quenching studies. Experiments were then performed to characterize and optimize microcombustion performance. A patent (Masel and Shannon, 2001) was issued on this microburner design.

Experimental

Two primary sets of experiments were performed: (1) quenching experiments were conducted to determine the roles that temperature and wall material play in radical quenching, and (2) microburner experiments where burners with submillimeter dimensions were constructed and tested to see whether stable combustion can be achieved and optimized. The work in all parts, unless specified otherwise, was done with methane–oxygen flames, whose mechanism is well understood.

During the quenching experiments, various candidate wall materials were mounted on aluminum or titanium blocks. The blocks were then mounted on an adjustable track so that the gap between the parallel wall materials could be manually adjusted. A standard methane/oxygen torch was placed below the blocks so that the flame would go through the gap between the walls. Then the distance between the walls was slowly reduced until the flame would not propagate through the gap between the walls. Gap distances were measured by viewing the gap separation between the plates with a 20× magnifying eyepiece. In the eyepiece's field of vision was a graduated ruler positioned to minimize parallax in the gap measurement.

The wall temperature was controlled by adding either a heat sink or an external heat source outside of the tested material's mounting blocks. Generally we either heated or cooled the blocks to maintain a constant inside wall temperature. Figure 1 shows a schematic of the wall region of the apparatus used to measure quench lengths. During the experiments, Type K thermocouples were used to measure the temperatures at T_1 and T_2 within the wall. The data were then used to extrapolate the temperature at T_S using the following equation

$$T_S = \frac{k_H}{k_S} \times \frac{L_S}{L_H} \times (T_1 - T_2) + T_1 \qquad (1)$$

where L_H is the thickness of the holder, k_H is the thermal conductivity of the holder, L_S is the thickness of the wall material, and k_S is the thermal conductivity of the wall material. Several materials were tested at two different conditions. Low surface temperature (near 500 K) tests were performed on quartz, stainless steel, copper, YSZ, and alumina. For these tests, the torch outlet was placed 8 mm below the bottom of the gap between the parallel plates. High surface temperature (near 1000 K) tests were performed on quartz, stainless steel, alu-

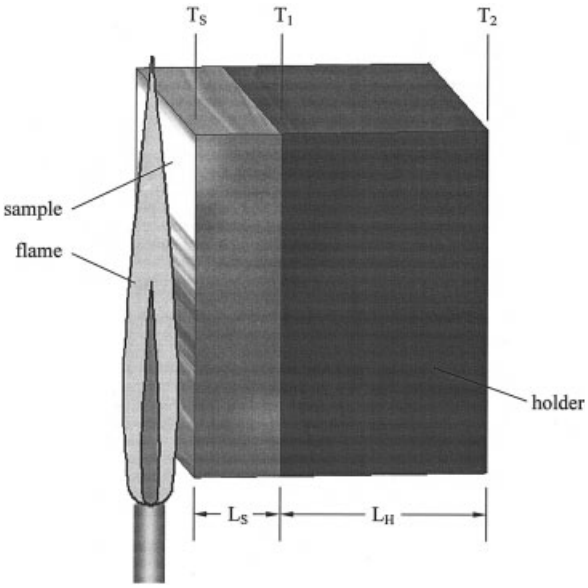

Figure 1. Wall region of the apparatus used to measure quench lengths.

During the experiments, Type K thermocouples were used to measure the temperatures at T_1 and T_2 within the wall. The data were then used to extrapolate the temperature at T_S using Eq. 1.

mina, and cordierite ($Mg_2Al_4Si_5O_{18}$) material that was pretreated to deplete the magnesia from the surface. We also attempted to do experiments on copper, but it oxidized. For these tests, the torch outlet was placed 32.5 mm below the bottom of the gap between the parallel plates.

Based on the results of these quenching studies and other material durability considerations discussed further in the Discussion section, polycrystalline alumina was chosen as the material for microburner construction. Three different styles of burners with a critical dimension of 0.75 mm were constructed by machining slots of different geometries in 40 × 10 × 1-mm polycrystalline alumina slides. All three burner configurations consisted of two machined slides juxtaposed after a surface preparation scheme was performed. The reaction zones for all three burner designs were of the same dimensions of 5 × 0.750 mm (cross section) × 35 mm (length).

The machined groove pattern for each of the three designs is shown in Figure 2, whereas the flow patterns are shown in Figure 3. Burner I was used in experiments with premixed gases. This burner had a 5-mm-wide slot machined into the entire length of two slides. The slot was 0.25 mm deep in one slide and 0.50 mm in the other. Premixed gases were fed to a tube on the bottom of the burner and the flame was stabilized with platinum gauze along the base of the burner.

Burner II was intended to house a laminar diffusion flame. The burner had a 5-mm-wide, 0.25-mm-deep Y-shaped slot machined into the first slide. An identical 0.5-mm-deep Y-shaped channel was machined into a second slide. Burner III, intended to house a laminar diffusion flame with a broader mixing layer, had a 5-mm-wide, 0.25-mm-deep slot machined into the first slide (see Figure 1). A 0.5-mm deep, identically shaped channel was machined into a second slide.

For all designs, after machining, the surfaces of the alumina

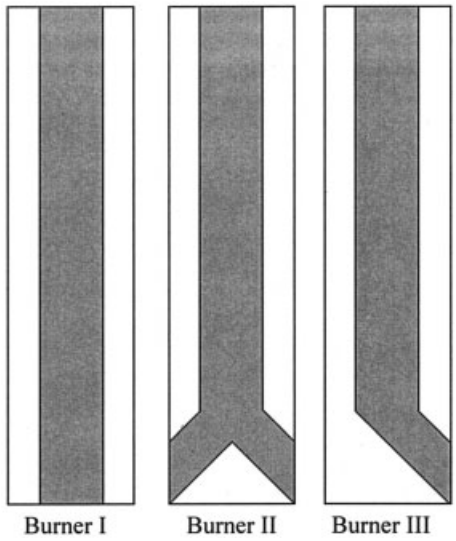

Figure 2. Machined groove pattern for each of the three burner designs.

Planar grooves (in gray) were machined into the broad side of a 40 × 10 × 1-mm polycrystalline alumina slide using a diamond-tipped end mill.

slides were treated by a three-step process developed to produce chemically inert surfaces on the reactor walls. First, to remove ionic and heavy metal contaminants from the surface, the slides were held at 80°C for 10 min in a bath of deionized water, concentrated hydrochloric acid, and 30% hydrogen peroxide at a 6:1:1 volume ratio. Slides were then annealed in an atmospheric environment at 1550°C for 1 h to reduce the existence of grain boundaries and other surface imperfections that would serve as quenching sites for radicals. Before the

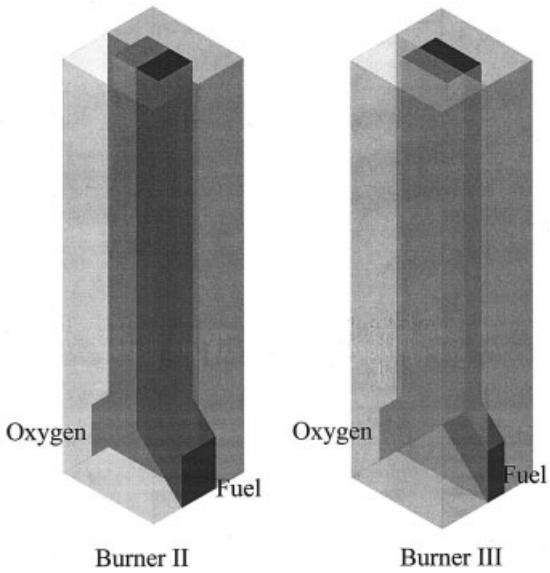

Figure 3. Flow pattern in the burner II and burner III for equal flow rates of fuel and oxygen and no combustion.

In the picture, the height and width are to scale, but the thickness of the slot was enhanced by a factor of 10 to make the flow pattern easy to see.

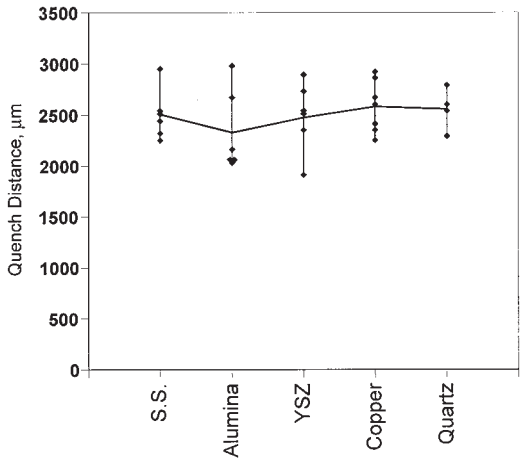

Figure 4. Quench lengths measured for a series of wall materials measured with outside wall temperatures near 300 K and inside wall temperatures below 500 K.

final surface preparation technique, the machined faces of the slides were juxtaposed and sealed along the edge with an alumina-based adhesive and mounted in a gas feed manifold made of alumina. For the premixed burner design (design I), a device to promote mixing of the fuel and oxidant was added in the manifold. For the diffusion flame burners, the manifold supplies gases to either inlet of the mixing channel, and has dimensions of 38 × 16 × 24 mm (length × width × height). The cavity into which the burner is mounted has dimensions of 13 × 5 × 16 mm (length × width × depth). The bottom 13 mm of the burners typically sits in the manifold. The microburner and manifold assemblies were then insulated in a layer of fibrous alumina insulation and heated to 1000°C for 12 h by resistive heating while oxygen is fed to the reaction chamber. This final step acts to further passivate the microcombustor's surface, thus reducing the potential for heterogeneous combustion reactions. SEM imaging verified the surface smoothing and grain boundary reducing effect of the high-temperature anneal.

In the laminar premixed flame burner (design I), the methane and oxygen are fed into a manifold where they are mixed before entering the submillimeter combustion channel. In the laminar diffusion flame burners (designs II and III), methane is fed into one leg of the microburner and oxygen is fed to the other. The mass flow controllers are 500 sccm (cm^3 at STP/min) for CH_4 and 1000 sccm for O_2 M100B models from MKS Instruments (Wilmington, DE). The listed accuracy of these instruments is ±1% of full range. The methane and oxygen react in the long sections of each burner. Products and unreacted supply gases are exhausted out of the top of the burner. Any unconsumed methane will mix with atmospheric air and may form a cone-shaped diffusion flame over the methane inlet side of the burner top. For burner design II, in all cases except one, this flame may be extinguished by gently blowing over the top of the burner, leaving the flame structure inside the burner unaltered. The exception is when a laminar diffusion flame is present in the channel, a structure that is found to occur in near limit conditions. In these cases blowing out the external burner top flame in turn extinguishes the internal diffusion flame, leaving a single flame cell near the inlet. For burner design III, no significant flame cone was present. Estimates of the Reynolds (Re) number based on the small gap dimension (0.75 mm) and typical injection rates are Re = 35–80 (cold flow conditions). The approximate Lewis (Le) numbers of methane and oxygen at 1000°C is 1.0. Type R thermocouples were attached to the outside surfaces of the burners with an alumina-based adhesive to monitor burner temperatures.

All luminosity images (see Figure 6 below) were taken with a Canon Powershot G1 camera and an IR cut filter lens. The camera was positioned over the top of the burner and angled to one side to view the flame cells that appear down the length of the burner. In all the flame luminosity images shown below, the base flame cell (that is, the flame cell closest to the burner inlet) is at the bottom of the images.

No preheating was necessary to achieve combustion in the burners. For all burner experiments, ignition was achieved by lighting the exhaust of the room temperature burner and letting the burner warm up.

Results

Quenching tests

Figure 4 shows the quench lengths measured for the low surface temperature (near 500 K) experiments. The data points show some scatter because they represent the quenching distances measured over the temperature range of 300 to 500 K and the quenching distance is temperature dependent. Notice that the quench lengths were relatively independent of wall composition, as one would expect if thermal quenching dominates. The data show an average quench length of 2.5 mm compared to 2.5 mm calculated by averaging the values in the work of Kondo et al. (1992), Fukuda et al. (1981), Ono and Wakuri (1977), and Maekawa et al. (1975).

Figure 5 shows results from the high surface temperature tests, where walls were externally heated so that the inside wall temperature of the slot started at 1000°C (temperatures were measured when the walls were 3 mm apart). In this case there

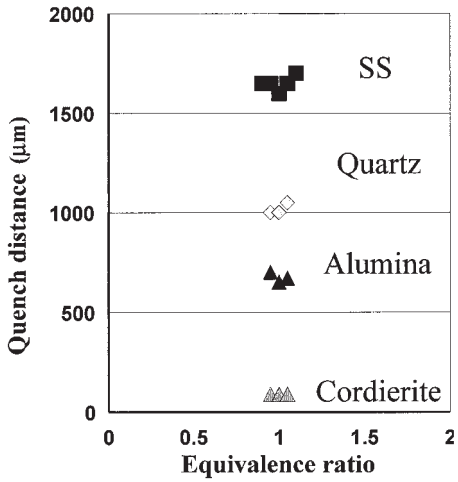

Figure 5. Quench lengths measured for a series of wall materials as a function of methane:oxygen ratio when the walls were insulated to give inside wall temperatures near 1000°C.

Table 1. Comparison of the Thermal Conductivities of Materials in Figure 5

Material	Thermal Conductivity ($W/m^{-1}/K^{-1}$) at 300 K	at 1000 K
Quartz*	1.38	2.87
Cordierite*	1.45	1.30
Alumina*	36	7.85
304 Stainless steel**	14	25

*Touloukian et al. (1970).
**Lide (1999).

is much less uncertainty in the data because the measurements were all done at a single wall temperature. Notice that the observed quenching distances vary strongly with the wall material. Stainless steel quenches the flame when the gap is reduced to 1.8 mm. In contrast, the flames seem to propagate through the cordierite walls when the gap is 100–200 μm. Commercial-grade alumina is somewhere in between. In supplementary experiments, it was found that the quench lengths of the quartz and alumina plates vary according to how the quartz or alumina was pretreated. In some cases, flames were able to propagate through a 200-μm gap between two alumina plates.

The implication of the results in Figures 4 and 5 is that when surfaces are colder, thermal quenching is the dominant flame quenching method. Quenching distances were a function, not of the material, but only of the wall temperature. If the radical chemistry or conduction in the wall were determining the quenching length, then one would expect the wall material to affect the quenching rate. The absence of an effect of the wall material suggests that heat transfer in the gas phase is determining the quenching distance, as one would expect if thermal quenching is dominant.

At higher temperatures, though, quenching distances become a function of surface material. We find that alumina and cordierite show the lowest quenching distances, whereas the quenching distances are higher with stainless steel and quartz. By comparison, Table 1 lists the published thermal conductivities of the materials. Note that quartz and cordierite have similar thermal conductivities over the entire range, whereas stainless steel and alumina have much higher thermal conductivities. A comparison between the quench data in Figure 3 and the thermal conductivity data in Table 1 shows that there is no correlation between the thermal conductivity of the walls and the quenching distance. The strong effect of the wall material on quenching and the absence of correlation between the quenching data and the thermal conductivity of the material is strong evidence that the thermal processes are not playing a key role in the quenching process. Also, we note below that surface preparation plays a key role in allowing flames to propagate. Therefore, we are suggesting that radical quenching must control quenching in this regime.

Microburner tests

Our early experiments were done on Microburner Design I. Premixed methane and oxygen were supplied to the bottom of the burner, and an attempt was made to verify combustion. Initial data were gathered with alumina as received, but no combustion was seen. However, after the burners were cleaned and annealed, sustained combustion was observed. Generally, burners with a 1-mm slot required an SC2 clean and high temperature anneal before they were able to sustain flames. One also had to do a high-temperature bake in an oxygen atmosphere to sustain flames in burners with 0.75- or 0.5-mm slots.

Once the walls were treated, sustained flames were routinely observed. Unfortunately, the gas temperature inside the burner reached a very high temperature near the entrance of the burner, which led to material failure.

To avoid the spatially concentrated release of heat, a second burner was designed to spread out the flame. The idea was to create a laminar flow pattern in Figure 3, where the mixing zone between the oxygen and the fuel was spread up the length of the reactor channel. Combustion in the mixing layer was expected to yield an elongated flame down the length of the channel, effectively spreading the exothermic release evenly down the burner's length.

Experiments at flow rates of 100 sccm CH_4 and 200 sccm O_2 (that is, stoichiometric) were used to test the idea. Again, untreated burners did not propagate flames and, again, burners with a 1-mm slot required an SC2 clean and high-temperature anneal before they were able to sustain flames. One also had to do a high-temperature bake in an oxygen atmosphere to sustain flames in burners with 0.75- or 0.5-mm slots.

The flame structure in the burners showed some unexpected behavior. Initially, while the burner is cold, a smooth laminar diffusion flame forms in the mixing layer between the fuel and oxidizer streams. A conical laminar diffusion flame is also typically present at the burner exit on the methane inlet side. It is formed when the excess methane that is not consumed inside the burner mixes with atmospheric air. Clearly a significant portion of the fuel is unconverted. Clearly we can have the diffuse flame we expected.

Surprisingly, though, the continuous diffusion flames were not stable in our burners. As the burner walls heat up, the diffusion flame inside the burner develops a distinct cellular structure along its length, before collapsing into three stationary, isolated flame cell structures.

Figure 6 shows the chemiluminescent emission from the different flame structures observed by pointing a camera down the burner slot. The camera was positioned over the top of the burner and angled to one side to view the flame cells that appear down the length of the burner. In all the flame luminosity images, the base flame cell (that is, the flame cell closest to the burner inlet) is at the bottom of the images. The figure shows photographs taken at several methane and oxygen flow rates. In the cases shown, one to four evenly spaced, nearly spherical flame cells were observed. All of these structures remained unaffected when the flame cone of exhausted methane with atmospheric oxygen was extinguished. A fifth structure, the expected continuous, elongated diffusion flame existed at certain feed conditions only when the exhaust cone was present. If the exhaust cone was extinguished while the noncellular elongated diffusion flame was present, the elongated flame was also extinguished, leaving only a single cell in the bottom (near the feed entrance) of the burner.

A series of experiments were performed with this burner to map the flame structures when the exhaust cone is extinguished as a function of total gas feed rate and equivalency ratio. The results of this are shown in Figure 7. Generally one can observe

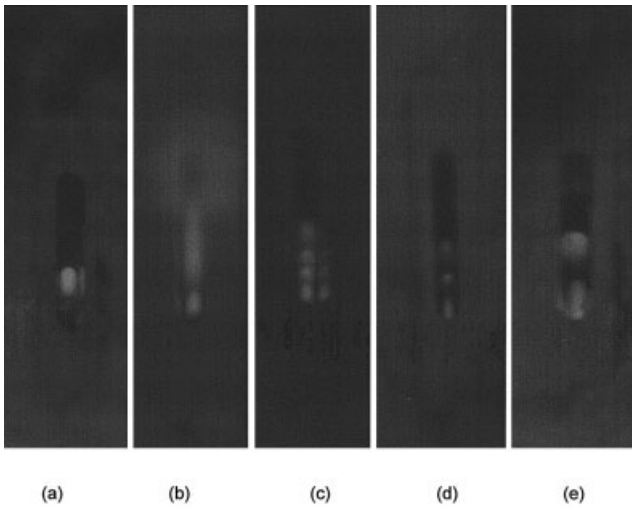

Figure 6. Chemiluminescent emission from burner design II.

(a) One flame cell present at a feed rate of 29 sccm CH_4 and 171 sccm O_2. (b) The laminar diffusion flame structure and isolated flame spot observed at a flow rate of 65 sccm CH_4 and 150 sccm of O_2. (c) Three flame cells present at a feed rate of 100 sccm CH_4 and 200 sccm O_2. (d) Four flame cells present at a feed rate of 100 sccm of CH_4 and 130 sccm of O_2. The smaller blue colorations slightly to the right of the more prominent flames are reflections of the true flames on the burner wall. (e) Two flame cells present at a feed rate of 67 sccm CH_4 and 266 sccm O_2. The images were taken with a Canon Powershot G1 camera and an IR cut filter lens. The camera was positioned over the top of the burner and angled to one side to view the flame cells that appear down the length of the burner. In all the flame luminosity images shown, the base flame cell (that is, the flame cell closest to the burner inlet) is at the bottom of the images. The variations in the background color are associated with variations in the room lighting.

from one to four flame cells in the burners. At low flow rates, one generally observes only one flame cell that sits near where the feed gases mix. As the flow rate increases, one starts to observe combustion all of the way up the burner, although the flame is not continuous. Instead one observes a series of four flame cells. The spacing between the cells increases as the flow rate inside the burner increases. Eventually the top cell moves out of the burner, so only three cells are seen.

A detailed analysis of the results shown in Figure 7 can be found in Miesse et al. (2004). Key observations are that decreasing the residence time or equivalency ratio generally decreases the number of observed flame cells. At sufficiently lower feed rates, combustion cannot be sustained. The position of the flame cells was instantly and predictably responsive to feed perturbations, possible along the entire length of the reactor, and aligned where the diffusion surface between the fuel and oxidant was expected to exist. This suggests that the cellular structure is not caused by inconsistencies in the burner surface's catalytic activity or temperature profile. To determine whether the stability of the segregated flame cells is a consequence of a Lewis (Le) number $\leq \sim 1$, analogous to the case in flameballs seen in microgravity by Ronney (2001), supplementary experiments were performed. Methane (Le = 0.9) was substituted with propane (Le = 1.7) as the fuel in the burner. Propane–oxygen laminar diffusion flames showed similar cellular flame structures. Methane was then substituted with a 95% hydrogen/5% methane fuel. The methane was added only to serve as a visual tracer because hydrogen combustion lacks the chemiluminescent emission associated with combustion of fuels with C—H bonds. The flame structure of hydrogen, with a Lewis number of 0.3, did not exhibit a cellular structure, but rather the expected tribrachial structure. Although hydrogen combustion proceeds faster than methane or propane combustion, the increased diffusion rate of hydrogen compared to that of methane and propane is even more significant. Hydrogen's diffusivity is more than an order of magnitude greater, which further suggests that mass transfer limitations are behind the formation of the cellular flame structures observed in hydrocarbon combustion in burner design II.

Outside wall temperatures were also measured during the experiments. Generally, the temperatures were a strong function of position along the burner's length. They varied from about 400 to 800 K, and the hotter regions were aligned with the flame cells on the inside of the burner channel. External wall temperature differences of about 70°C were possible in distances of 2 mm in the axial direction.

Burner design II was operated continuously for weeks with

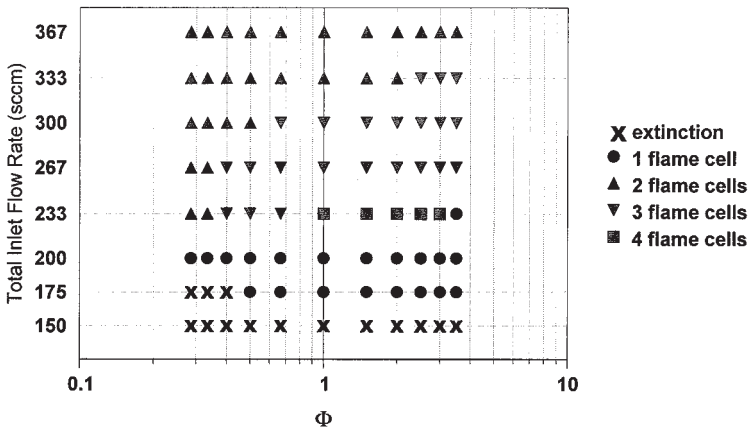

Figure 7. Flame structure observations of the combustion structure inside the burner with the cone flame extinguished.

no noticeable performance degradation. Thus it is an acceptable burner design.

The final burner design, burner III, is shown in Figure 2. It was designed to create the flow pattern in Figure 3 where there is a much larger diffusion surface between the fuel and oxidant. With this design, diffusion times are much lower than those in burner II. Burner III was tested using the same procedures as in burner II, but the results were quite different. In this design, the cellular instabilities did not exist. Rather, an intense flame existed throughout the reactor channel. The outside wall temperature for this burner was about 1500 K (measured in the middle of the broad side of the 0.5-mm slide) at a flow rate of 100 sccm methane and stoichiometric oxygen, dramatically higher than the temperatures observed in design II. The alumina burner glowed orange when operated. No significant external cone was present with this burner design, suggesting that fuel conversion approached 100%. Burner design III was operated continuously for weeks with no noticeable performance degradation.

Discussion

Quenching measurements

The results here show that heat transfer and wall quenching each play a critical role in flame propagation on the microscale. The quenching experiments were designed to make two determinations. The first was to determine the relative roles of thermal and radical quenching in microscale flame quenching. The second was to determine the effect of surface composition and material properties on radical quenching.

We conclude that at low temperatures thermal quenching dominates, whereas at higher temperatures, the radical quenching plays a dominant role. The burner studies show that the surface preparation of the material plays an important role in the quenching process. Annealing the surface in oxygen was essential for allowing flames to propagate through the smallest burners. The annealing process does not affect the thermal properties of the materials, but it does eliminate radical traps (oxygen vacancies) from the surface. Thus, it is clear that heterogeneous radical quenching is playing an important role in this temperature regime. Also, there is no correlation between the measured quenching distance and the thermal conductivity of the material. Thus thermal quenching seems to be less important in this temperature regime.

It is useful to compare our results with those from the previous literature. Friedman and Johnson (1950), Westbrook et al., (1981), Sloane and Ratcliffe (1982), and Sloane and Schoene (1983), measured quenching distances at surface temperatures from 373 to 800 K. They each concluded that heterogeneously catalyzed radical recombination does not play a significant role compared to that of thermal quenching. The quenching measurements (Figure 4) that were performed at lower temperatures agreed with the findings of the earlier research performed at lower temperatures, specifically, that at lower temperatures thermal quenching is the dominant flame-quenching mechanism.

More recent computational work by Vlachos et al. (1994) predicts that at higher surface temperatures, heterogeneous effects are significant. In part, this should be expected because the near-wall temperatures will be higher than those in earlier studies, heat losses will be less, and the relative rates of combustion propagation reactions to homogeneous radical recombination terminations will not be decreased as severely.

Our high surface temperature experiments agree with the trend predicted by computations of Vlachos and coworkers for burners with walls that quench radicals. Figure 5 shows that at elevated surface temperatures, quenching distances become strong functions of surface composition and do not correlate with thermal conductivity. Surface preparation to eliminate radical traps is essential to obtaining small quenching distances. Thus, heterogeneous radical quenching is dominant in this temperature regime. This is a significant result that implies that under proper thermal conditions, careful attention to surface composition can enable propagation of homogeneous combustion of hydrocarbons in gap sizes smaller than the quenching distances published in standard references, often considered the fundamental limitation.

Clearly from the results in Figure 5, the materials of construction chosen for surfaces in a microburner will have a great influence on its success in flame propagation. Stainless steel and alumina both have similar thermal conductivities, but stainless steel rapidly quenches flames, whereas flames pass through 0.5-mm alumina burners. The difference in the thermal conductivity of the materials is insufficient to account for this difference, but the differences in the trapping of radicals could account for the effect. Iron, chromium, nickel, and their oxides form strong bonds to hydroxyls. According to Masel (1996), stainless steel should rapidly quench the hydroxyls in a typical flame. In contrast, alumina should form a strong bond only at defects and possibly at impurities (see Masel, 1996). Thus, defect-free alumina is expected to be fairly inert with respect to heterogeneous radical recombination. Experimentally, we find that alumina as received quenches flames, but flames propagate through properly treated 0.5-mm alumina burners. A three-step cleaning process is needed to get flames to propagate: first an SC2 clean to remove transition metal impurities, then a high-temperature anneal in vacuum to remove steps, and finally an oxygen bake to remove oxygen vacancies. This is as expected if radical quenching controlled the rate. In contrast, if thermal quenching controlled the rate, then the heat treatment of the alumina should not make any difference to the flame propagation, and alumina and stainless steel should show similar results. Clearly, alumina and stainless steel were different, which is strong evidence that radical quenching plays an important role.

Alumina was not the best material we found to propagate flames. Instead cordierite that was pretreated to deplete the magnesia from the surface showed the smallest quenching rate. The cordierite lattice has very few of the Lewis acid defects that would be expected to rapidly quench hydroxyls. Magnesia was depleted from the surface of cordierite to eliminate a direct reaction between the magnesia and hydroxyls from the homogeneous phase to further reduce radical quenching. This material proved to have the lowest ability to quench flames. Unfortunately, it also had a tendency to melt in the burners.

Burners

The results here show that one can build robust microburners with proper design, but the wall materials, pretreatment, and the flow pattern design are critical to the success. Burner design I, for example, was not initially able to pass flames. However,

flames would propagate after the walls were treated. Unfortunately, the burner was not robust. The reaction appeared to go to completion near the burner entrance, concentrating the exothermic energy release in a small area. It is suspected that the premixed nature of the feed allowed the reaction zone to approach the adiabatic flame temperature of stoichiometric methane–oxygen combustion, 3030 K (Glassman, 1996). This is considerably higher than the melting point of polycrystalline alumina, 2323 K (Munro, 1997). This result shows that one needs to be very careful in designing the flow pattern for microburners. It is important to avoid hot spots that would degrade the materials.

To prevent the spatially concentrated heat release exhibited in burner I, the flow pattern in burner II was created to produce a diffusion plane between the fuel and oxidant that extended across the length of the burner, as shown in Figure 3. Ideally, combustion would occur along the diffusion plane, where the reactants are sufficiently mixed. This burner worked in the sense that flames propagated and the walls survived, but the combustion was incomplete. We had hoped for a typical tribrachial flame structure with nearly complete combustion. However, in most cases, an array of segregated flame cells was observed. Possible explanations of this novel flame structure are proposed elsewhere (Miesse et al., 2004). Generally, in a high aspect ratio flow, diffusion of reactant species into the reacting mixing layer from the edges of the burner is slow compared to reaction rates, which produces a cellular instability. Because of mass transfer limitations, only about 5–25% of the entire burner volume is actually occupied by vigorous combustion. This is unacceptable for a device where space efficiency is an objective.

The burner design III was a compromise between designs I and II. Burner III retained the diffusion flame characteristic, but had a more efficient contacting pattern for the fuel and oxidant. To increase the area of the reacting mixing layer, the fuel and oxidant were added such that the resulting mixing layer spanned the length and width of burner, as shown in Figure 3, yielding a reacting mixing layer that is about 35×5 mm, compared to the previous design's reacting mixing layer size of about 35×0.75 mm. The position of the mixing layers of the two laminar diffusion burners can be visualized by considering the laminar flow pattern resulting from the schematic of the burner halves shown in Figure 3. In addition to a nearly sevenfold increase ($5 \text{ mm} \div 0.75 \text{ mm}$) in the reacting surface, the diffusion lengths of burner design III are significantly shorter than those in burner design II. For complete combustion to occur in burner II, pure fuel from one side of the 5-mm-wide channel must diffuse to the oxidant diffusing from the other side of the channel before exiting the reactor channel. The cellular flame structure present in design II demonstrates that this diffusion process is too slow for acceptable conversion. Burner design III reduces the gap across which the pure species must diffuse to complete combustion from 5 to 0.75 mm, substantially reducing the diffusion time required for complete conversion. The highly elevated temperatures and, more important, the lack of any significant cone at the exhaust of burner Design III suggests that the improved contacting pattern of fuel and oxidant yielded the near 100% conversion typical of conventional combustion reactors. At the same time, despite the high conversion, the reaction was spread over the length and width of the microburner, preventing the material failure observed in design I, which also had a high conversion.

Conclusions

The quenching tests demonstrated that for cold walls, thermal quenching is the dominant flame-quenching mechanism. However, as wall temperature approaches combustion temperatures, heterogeneously catalyzed radical recombination controls flame quenching.

The results show that there are three keys to successful microburner design: (1) the device needs to be insulated well enough that the heat of combustion is sufficient to keep the reacting mixture hot enough to sustain significant combustion and prevent thermal quenching; (2) the walls of the microburner need to be fabricated from materials that do not quench radicals so that the gas-phase combustion reactions can occur unimpeded; and (3) the flow pattern in the burner needs to be such that the temperature is low enough not to melt the walls, yet the flame fills the entire space. Microburner design III gave the highest efficiency, and highest conversion in our experiments. The results here clearly demonstrate that hydrocarbon combustion can be achieved in submillimeter combustion cavities with careful burner design.

Acknowledgments

This work was supported by Dyncorp Grant DABT63-98-1-0157 under DARPA contract DABT63-95-C-0114 and by the Army Research Office under contract DAAD19-01-1-0582. Any opinions, findings, and conclusions or recommendations expressed in this publication are those of the authors and do not necessarily reflect the views of Dyncorp, DARPA, or the Army Research Office. The authors thank Nicholas Ndiege, Anthony Chiu, and Min Young Chong for assistance in taking data for Figure 7.

Literature Cited

Aghalayam, P., P. A. Bui, and D. G. Vlachos, "The Role of Radical Wall Quenching in Flame Stability and Wall Heat Flux: Hydrogen–Air Mixtures," *Combust. Theory Model.*, **2**, 515 (1998).

Davy, H., "Some Researches on Flame," *Trans R. Soc. Lond.*, **45** (1817).

Dagaut, P., J. C. Boettner, and M. Cathonnet, "Methane Oxidation: Experimental and Kinetic Modeling," *Combust. Sci. Technol.*, **77**, 127 (1991).

Fernandez-Pello, A. C., "Micropower Generation Using Combustion: Issues and Approaches," *Proc. Combust. Inst.*, **29**, 883 (2002).

Friedman, R., and W. C. Johnson, "The Wall-Quenching of Laminar Propane Flames as a Function of Pressure, Temperature, and Air-Fuel Ratio," *J. Appl. Phys.*, **21**, 791 (1950).

Fukuda, M., K. Korematsu, and M. Sakamoto, "On Quenching Distance of Mixtures of Methane and Hydrogen with Air," *Jpn. Soc. Mech. Eng.*, **24**, 1192 (1981).

Glassman, I., *Combustion*, 3rd Edition, Academic Press, San Diego, CA (1996).

Jensen, C. D., "The Dependence of Flame/Wall Interactions on the Composition of the Walls for Determining the Material Composition of a Micro-Combustor," MS Thesis, University of Illinois at Urbana–Champaign (2000).

Jensen, C. D., R. I. Masel, G. V. Moore, and M. A. Shannon, "Burner Designs for Microcombustion," *Combust. Sci. Technol.*, **00**, 000, 2003.

Ju, Y., H. Guo, K. Maruta, and F. Liu, "On the Extinction Limit and Flammability Limit of Non-Adiabatic Stretched Methane–Air Premixed Flames," *J. Fluid Mech.*, **342**, 315 (1997).

Klein, J., C. Lettmann, and W. F. Maier, "Thermally Stable, Silica-Based Amorphous Porous Mixed Oxides Prepared by Sol–Gel Procedures," *J. Non-Cryst. Solids*, **282**, 203 (2001).

Kondo, S., S. Horiguchi, M. Iwasaka, K. Tokuhashi, and H. Nagai, "Effect of Pressure and Oxygen Concentration on Quenching Distances of Flammable Gases," *Nippon Kagaku Kaishi*, **7**, 788 (1992).

Kuo, K. K., *Principles of Combustion*, Wiley, New York (1986).
Lide, D. L., *Handbook of Chemistry and Physics*, CRC Press, New York (1999).
Lucquin, M., "The Controlled Combustion of Methane at Low Temperature," *J. Int. Combust. Convers. Energie* (*Paris*), **45**, 9 (1964).
Maekawa, M., "Flame Quenching by Rectangular Channels as a Function of Channel Length for Methane–Air Mixture," *Combust. Sci. Technol.*, **11**, 141 (1975).
Masel, R. I., *Principles of Adsorption and Reaction on Solid Surfaces*, Wiley, New York (1996).
Masel, R. I., *Chemical Kinetics and Catalysis*, Wiley, New York (2001).
Masel, R. I., and M. A. Shannon, "Microcombustor Having Submillimetric Dimensions," U.S. Patent No. 6 193 501 (2001).
Miesse, C. M., R. I. Masel, M. A. Shannon, and M. Short, "Experimental Observations of the Structure of a Diffusion Flame in a Sub-Millimeter Microburner," *Combust. Theory Model.*, (2004).
Moore, G., "Failure of a Thin-Film Mullite Synthesis due to Carbothermic Reduction by the SiC," MS Thesis, University of Illinois at Urbana–Champaign (2000).
Munro, R. G., "Evaluated Material Properties for a Sintered alpha-Al_2O_3," *J. Am. Ceram. Soc*., **80**, 1919 (1997).
Ono, S., and Y. Waurika, "An Experimental Study on the Quenching of Flame by Narrow Cylindrical Passage," *Bull. Jpn. Soc. Mech. Eng.*, **20**, 1191 (1977).
Ronney, P. D., "Premixed-Gas Flames," *Microgravity Combustion: Fires in Free Fall*, H. Ross, ed., Academic Press, London (2001).
Sloane, T. M., and J. W. Ratcliff, "A Molecular Mean Mass Spectrometer Study of Side-Wall Flame Quenching at Low Pressure by Cooled Non-Catalytic and Catalytic Surfaces," *Combust. Flame*, **47**, 83 (1982).
Sloane, T. M., and A. Y. Schoene, "Computational Studies of End-Wall Flame Quenching at Low Pressure: The Effects of Heterogeneous Radical Recombination and Crevices," *Combust. Flame*, **49**, 109 (1983).
Touloukian, Y. S., R. W. Powell, C. Y. Ho, and P. G. Klemens, "Thermal Conductivity," *Thermophysical Properties of Matter*, Vols. 1 and 2, Plenum Press, New York (1970).
Vlachos, D. G., L. D. Schmidt, and R. Aris, "Ignition and Extinction of Flames Near Surfaces: Combustion of CH_4 in Air," *AIChE J.*, **40**, 1005 (1994).
Westbrook, C. K., A. A. Adamczyk, and G. A. Lavoie, "A Numerical Study of Laminar Flame Wall Quenching," *Combust. Flame*, **40**, 81 (1981).

Manuscript received Oct. 28, 2003, and revision received Mar. 31, 2004.